General considerations

All air- and moisture-sensitive manipulations were carried out using standard vacuum line Schlenk techniques or in a M Braun dry-box containing an atmosphere of purified argon. Elemental analyses were performed at the Mikrolabor of ETH Zürich. UV/vis spectra were recorded on an UV/vis/NIR lambda-19-spectrometer (range 200-600 nm) in 10 mm Quartz cells. Mass spectrometry measurements were carried out by the MS Service (Laboratory of Organic Chemistry) at ETH Zürich. The melting points were determined with a Büchi M-560 device.

Materials

Cellulose nanocrystals obtained from wood pulp by sulfuric acid treatment were provided by the University of Maine. They were purified by Soxhlet extraction with ethanol for 24 h before modification.[1] Poly(ethylene glycol) methyl ether methacrylate (M_n = 950 g/mol) was purchased from Sigma-Aldrich (Switzerland) and used directly. Brilliant green dye was obtained from Merck (Germany). DME, DMF, THF, n-hexane, diethyl ether and toluene were degassed and purified using an Innovative Technologies PureSolv system. Standard chemicals were purchased from ABCR, Acros, Aldrich and Fluka or provided by BASF Switzerland. Deionized water was used in all experiments.

Synthesis of 2-hydroxyethyl 3-(bis(2,4,6-trimethylbenzoyl)phosphoryl)propanoate (3, BAPO-HEA)

A solution of bis(mesitoyl)phosphane (13.06 g, 40 mmol, 1 eq.) and triethylamine (0.56 mL, 4 mmol, 0.1 eq.) in DME (100 mL) was prepared in a 250 mL Schlenk flask. 2-Hydroxyethyl acrylate (4.3 mL, 40 mmol, 1 eq.) was added. After stirring for 12 h at room temperature, the solvent was removed under reduced pressure. The yellow oily residue was dissolved in toluene (80 mL) and aqueous hydrogen peroxide (7.9 mL, 80 mmol, 2 eq., 35%) was added dropwise at 0 °C. After stirring vigorously at r.t. for 6 h, the solvent was removed under reduced pressure. After recrystallization from diethyl ether/pentane (80 mL/30 mL, -20 °C), a yellow powder was obtained after removing the solvent under high vacuum for 14 h (16.42 g, 89.5%).

Synthesis of 2-([{6-isocyanatohexyl}carbamoyl]oxy)ethyl 3-(bis(2,4,6-trimethylbenzoyl) phosphoryl)propanoate (5, BAPO-NCO)

A solution of hexamethylene diisocyanate (11.7 mL, 72 mmol, 3 eq.) and catalytic amounts of DBTDL (200 µL, 1.3 mol%) in 30 mL THF was prepared in a 250 mL Schlenk flask. BAPO-HEA (11.00 g, 24 mmol, 1 eq.) dissolved in 60 mL THF was added dropwise at room temperature. After stirring for 16 h at 50°C in the dark, the reaction mixture was concentrated to 30 mL and precipitated in 150 mL hexane. The yellow precipitate was filtered off and recrystallized from diethyl ether/hexane (30 mL/ 10 mL, r.t. to -20°C, 20 h). A yellow solid was obtained after removing the solvent under high vacuum for 14 h (14.03 g, 93.2 %).

Synthesis of CNC-BAPO

In a 500 mL Schlenk flask, 3.0 g (18.5 mmol) neat cellulose nanocrystals were dispersed in 150 mL dry DMF before ultra-sonication (35 kHz) at 0 °C for 30 min. Subsequently, 12.5 g (20 mmol, 1.1 eq.) BAPO-NCO and a catalytic amount of DBTDL (500 µL, 4 mol%) dissolved in 20 mL dry DMF were added. The suspension was heated to 100 °C and stirred for 24 h under argon in the dark. After the reaction was completed, the suspension was centrifuged and the modified cellulose nanocrystals were subsequently washed with acetone in a Soxhlet extractor for 24 h. The purified CNC-BAPO was suspended in H_2O (0.05 g/mL) and stored in the fridge and in the dark. Elementary analysis [found %]: C, 46.79; H, 6.66; N, 2.53; S, 0.76; P, 0.94. The final weight of dry CNC-BAPO, measured gravimetrically by drying an aliquot of the water suspension, was 3.6 g. The value correlates well with the elementary analysis, which gives 3.7 g.

Preparation of formulations

A weight of 20 g for each formulation (Table 1) was prepared. PEGMEM was dissolved in water first, followed by adding photoinitiators and cellulose nanocrystals. Suspensions containing cellulose nanocrystals were homogenized using an Ultra-turrax stirrer (IKA, T10) for 10 min in the dark. The homogenized suspension was degassed at a reduced pressure.

Photopolymerization kinetics and rheological characterizations

Rheological measurements in real time were performed using an Anton Paar rheometer (Physica MCR 302) in parallel plate mode. For photorheology tests the light source used was a Hamamatsu LC8 lamp with a bulb emitting visible light (15 mW/cm^2) and a cutoff filter below 400 nm equipped with a 7 mm light guide. The set-up has a lower plate in quartz, the gap between the two plates was set to 0.1 mm and the sample was kept at a constant temperature (25 °C). Under a constant shear frequency of 60 rad/sec, light was turned on after 1 min in order to stabilize the system. Concomitant changes in viscoelastic material moduli (*G'* and *G"*) during illumination were measured as a function of exposure time. The measurements were carried out in the linear viscoelastic region (strain amplitude 0.1%).

For the frequency and amplitude sweep tests the formulation were placed on the quartz plate, the gap was set at 0.1mm and the material was cured for 4 minutes. Frequency sweep tests were performed over a frequency range of 0.1-100 rad/sec and with a constant strain amplitude of 1%. Amplitude sweep tests were performed over a strain range of 0.1-10000% at a constant frequency of 10 rad/sec.

Preparation of thin films

Thin films (0.5 mm thick) were prepared by casting the formulations in a plastic mold and irradiating 2 min with visible light (Hamamatsu LC8, 25 mW/cm^2) under nitrogen atmosphere. All samples were dried for 2 days in vacuum at room temperature before removing from the mold.

Dynamic mechanical analysis and tensile test

Thin films were cut into rectangle-shaped specimens with a length of 30 mm, a width of 5 mm. The measurements were performed with a Triton Technology TTDMA in tensile configuration. All experiments were performed with a temperature ramp of 3 °C/min, applying a force with a frequency of 1 Hz and with 10 µm of displacement. The same equipment was used for performing tensile tests on printed samples (30 mm length, 5 mm width, 4 mm thick) in controlled-force mode (force increase 0.5 N/min). 4 specimens were tested for each composition to give the average Young's modulus (*E*) values. The mechanical experiments were carried out at 25 °C both on dried samples and on samples after 5h of swelling in water.

Calculation of Crosslinking density

The crosslinking density is calculated from the measured storage modulus (*E'*) values above T_m, according to the statistical theory of rubber elasticity.[2] The number of moles of crosslinking points per unit volume, i.e. the crosslinking density for a network can be obtained from the equation: $E' = \nu RT$, where ν is the crosslinking density, R is the universal gas constant, and T is the temperature.

3D printing of model structures

Three-dimensional hydrogels were printed by UV-curing the formulations containing CNC-BAPO (**III** and **IV**). Brilliant green dye (0.05 wt% of the monomer) was used to limit the light penetration. The predesigned digital models were 3D printed using a Freeform Pico Plus 39 DLP printer (Asiga) with XY pixel resolutions of 39 microns using a UV-LED light source (405nm, 22 mW/cm^2). The layer thickness was settled at 20 µm and the layer exposition time varied from 3 to 6 seconds according to the design. After printing, the structures were rinsed with water in a sonicator for 3 min to remove residual non-cured materials. A subsequent post curing process was performed with a medium pressure mercury lamp for 5 min (provided by Robot Factory).

Nanoindentation tests

Hardness (H) and reduced elastic modulus (E_r) were performed using the NanoIndenter Ti950 (Hysitron) with a higher load head (3D OmniProbe) designed to accommodate a wide range of applications. The tests were performed by applying and removing controlled loads to the specimens using a geometrically well-defined probe.[3] A cono-spherical probe was used. Conical-spherical probe is a conical shaped probe with a spherical end (with a radius of 5 µm). Three different loads (3 mN, 10mN and 20 mN) are used to test the dried samples on the XY axis plane. The swollen samples were tested only with a load of 3 mN. Because if higher loads are used, the depth is over of instrument limits. The dried samples are also tested in Z surface with a load of 10 mN. To test the homogenity of hardness along the depth, the indentation on Z axis plane were realized at the distance of 190 µm. The loads were applied with a rate of 0.25 mN/s with a permanence time at the maximum load of 5 s. The swollen samples were valued in terms of maximum depth (h_{max}), because the depth is extremely high in relation to the load and the hardness value is not reliable. It is clear that the samples with a maximum depth have the highest resistance to penetration.

Swelling kinetics

The swelling kinetics of the gels in PBS was measured gravimetrically at room temperature. The vacuum dried samples were immersed in PBS. At different time intervals, the hydrogels were removed from the solution and the weight was determined after wiping off the liquid on the surfaces with wet filter papers. The swelling ratio (SR) is defined as follows $SR = 100 \times (W_t - W_d)/W_d$, where the W_t is the weight of the hydrogel at a certain time and W_d in the weight of the dried hydrogel.

Solution NMR spectroscopy

^{1}H, ^{13}C, ^{31}P NMR spectra were recorded on Bruker 300 spectrometer operating at 300.13 MHz, 75.47 MHz and 121.49 MHz, respectively. Chemical shifts δ were measured according to IUPAC and are given in parts per million (ppm) relative to TMS and H_3PO_4 for ^{1}H, ^{13}C and ^{31}P respectively.

Infrared Spectroscopy (FTIR-ATR)

FT-IR spectra of the dried samples were recorded using a Tensor 27 FT-IR spectrometer (Bruker, Switzerland). For each sample, the diamond crystal of an Attenuated Total Reflectance (ATR) accessory was brought into contact with the area to be analyzed. The contact area was a circle of about 1.5 mm in diameter. All spectra were recorded between 4000 and 600 cm^{-1} with a resolution of 4 cm^{-1} and 32 scans per sample.

Atomic-force microscopy (AFM)

The AFM measurements were performed on a commercial AFM system (BioScope Catalyst, Bruker Nano, Santa Barbara, California) that is mounted onto an inverted confocal laser-scanning microscope (FluoView FV500, Olympus, Center Valley, Pennsylvania). 10 µL of diluted aqueous suspension (0.001 wt%) of each sample was deposited onto freshly cleaved mica and left to dry at room temperature. The height images were obtained using tapping mode AFM with ATEC NC cantilever probes (Nanosensors, Neuchatel, Switzerland). The images are 2 x 2 µm in size, with a resolution of 512 x 512 pixels, and a scan rate of 0.5 Hz was used.

Solid-state ^{13}C and ^{31}P CP-MAS NMR spectroscopy

Solid-state ^{13}C and ^{31}P CP-MAS NMR spectra were recorded at RT on a Bruker Avance 400 NMR spectrometer (Bruker BioSpin AG, Fällanden, Switzerland) using a 4 mm CP-MAS probe. Approximately 30 - 40 mg of dried material was packed in a 4 mm zirconia rotor. The ^{13}C and ^{31}P CP-MAS NMR spectra were recorded at 100.6 and 162.0 MHz, respectively, using the following parameters: 3.5 µs 90° excitation pulse on ^{1}H channel, 3 ms contact time with a ramp from 100 to 50% of power level on the proton channel, 10,000 (^{13}C) and 13,000 Hz (^{31}P) MAS rates, 4 s relaxation delays, 71 kHz SPINAL 64 proton decoupling

was applied during acquisition, and appropriate numbers of scans were recorded to yield reasonable signal-to-noise ratios.

X-ray Diffraction Analysis (XRD)

XRD measurements of all samples were performed using a Bruker D8 Advanced diffractometer (Cu Kα radiation: *l* = 1.54184 Å; tube parameters: V = 40 kV, I = 40 mA) with a parallel incident beam prepared by a Göbel Xray mirror. The patterns were recorded with a 1D position sensitive detector (VÅNTEC). The powder samples were measured using a flat sample holder in reflection mode. The scans were recorded in the 2θ range 5–40°.

Thermogravimetric Analysis (TGA)

TGA analyses were conducted by using a TGA7 apparatus (PerkinElmer, USA). The dried samples (~5 mg) were heated from 30 to 800 °C at a constant rate of 20 °C/min under a He atmosphere.

Differential scanning calorimetry (DSC)

DSC analyses were performed using a Netzsch DSC 204 F1 Phoenix instrument, equipped with a low temperature probe. The experiments were carried out between -50 and 100 °C with a scan rate of 10 °C min^{-1}.

Gel content determination

The insoluble fraction (gel content) of the products was determined according to the following procedure: the samples were held in a metal net, weighted and subsequently submitted to extraction for 24 hours at room temperature in water to dissolve the non-cross-linked polymers. Then the samples were dried for 2 days in vacuum at room temperature. The insoluble fraction percentage was determined as weight difference before and after solvent extraction.

Determination of swelling ratio

The thin films were immersed in deionized water for 24 h at room temperature. Then, the samples were removed from the water and blotted dry to gently remove excess water. The swollen sample mass was recorded. Afterwards, the hydrogels were dried for 2 days in vacuum at room temperature and then the dry mass was recorded. 3 specimens were tested for each composition. The swelling percentage of the cross-linked samples was calculated as:

$$Swelling(\%) = \frac{W_s - W_d}{W_d} \times 100\,;$$

W_d = Weight of dry sample, W_s = Weight of swollen sample.

Focused Ion Beam Scanning Electron Microscopes (FIB-SEM)

The samples were mounted with conductive Silver paint on aluminium SEM-stubs and were sputter coated with 2 nm Iridium while rotating. Perpendicular cross section milling was performed in a FEI Helios 600i FIB-SEM with a Gallium ion beam at 30 kV and 2.5 nA. Polishing was done at 30 kV and 790 pA. The polished cross section was imaged with an electron beam at 2 kV and 0.17 nA by detecting backscatter and secondary electrons (through-the-lens detector in different detection modes: TLD BSE, TLD SE).

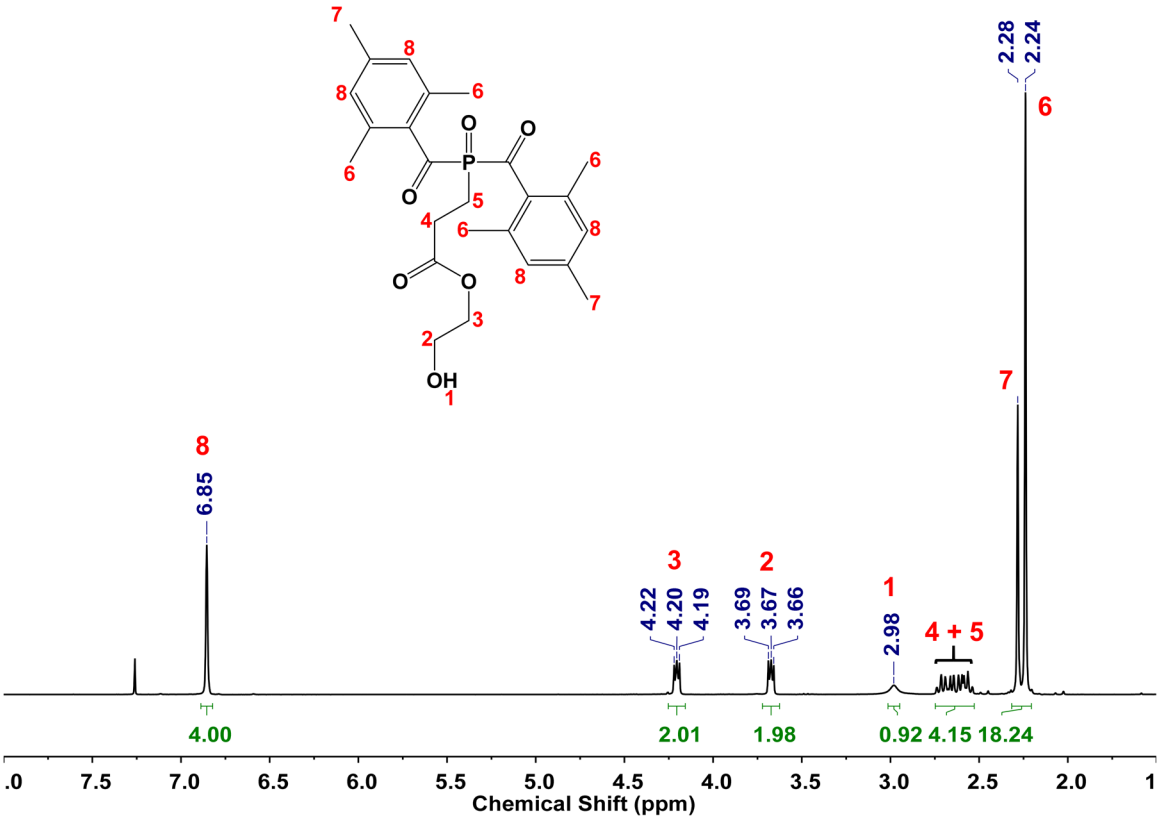

Figure S1a. ^{1}H NMR spectrum of BAPO-HEA (**3**) in $CDCl_3$.

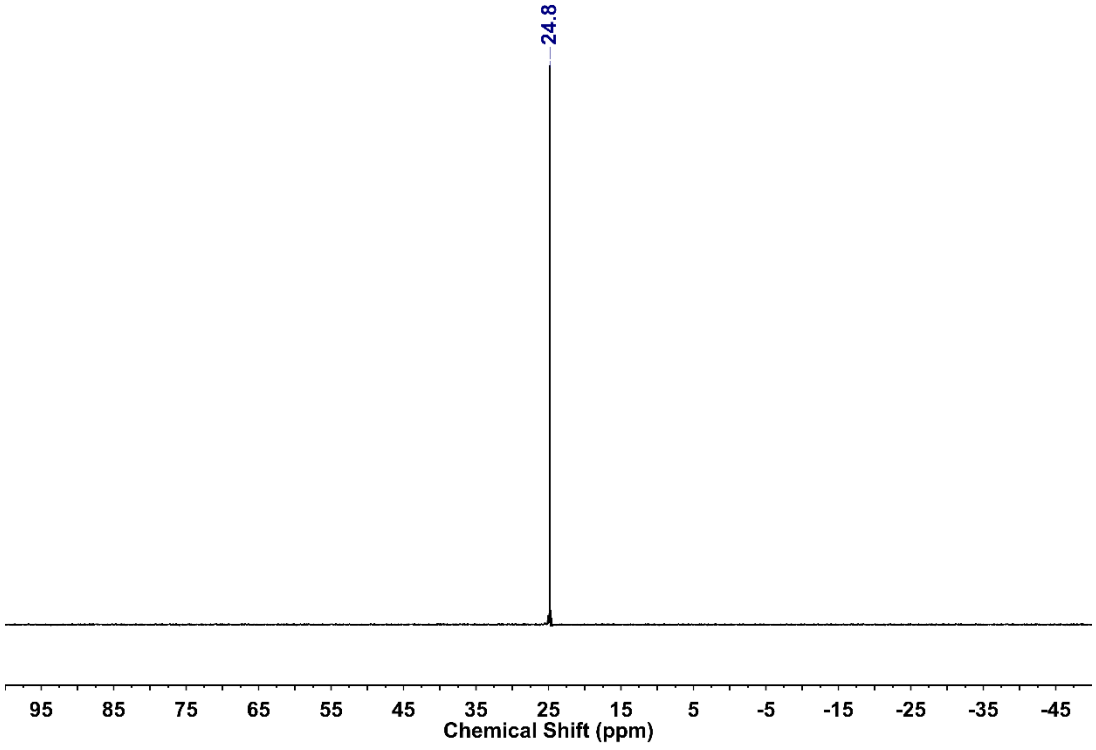

Figure S1b. $^{31}P\{^{1}H\}$ NMR spectrum of BAPO-HEA (**3**) in $CDCl_3$.

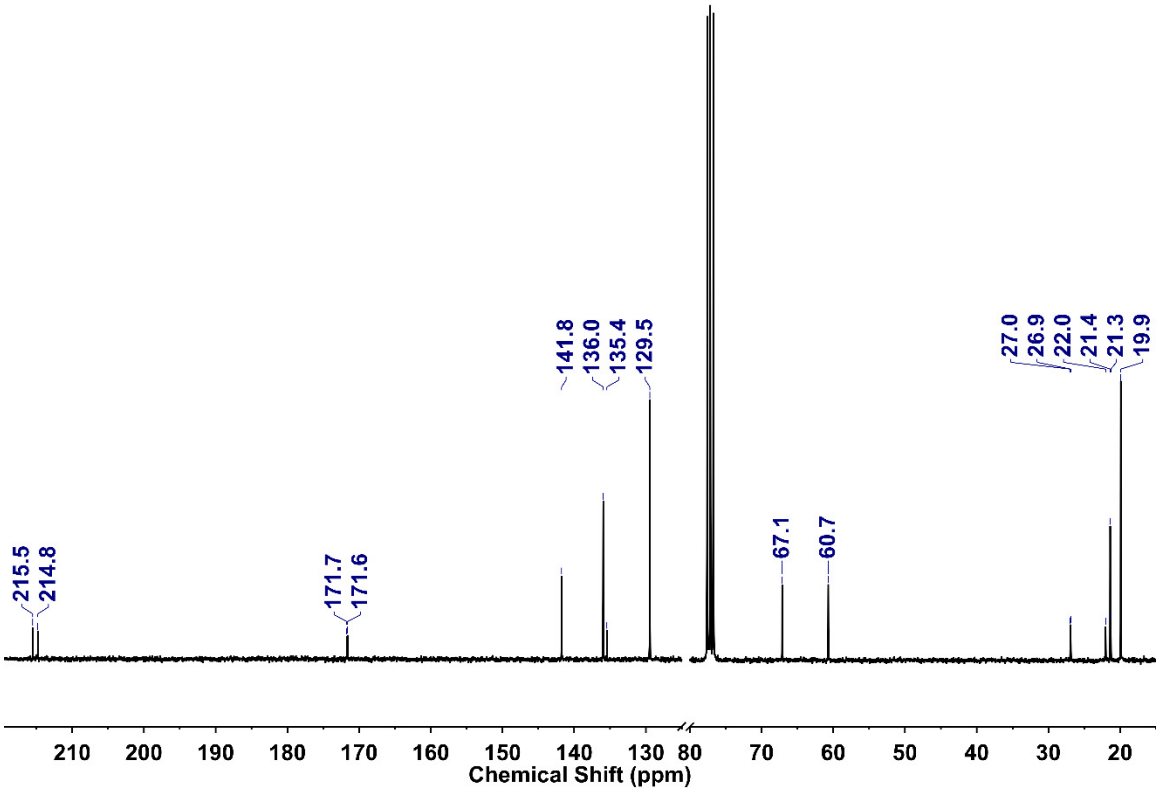

Figure S1c. $^{13}C\{^{1}H\}$ NMR spectrum of BAPO-HEA (**3**) in $CDCl_3$.

Characterization of 2-hydroxyethyl 3-(bis(2,4,6-trimethylbenzoyl)phosphoryl)propanoate (3)

^{1}H NMR (300.13 MHz, $CDCl_3$, 298 K): δ [ppm] = 2.24 (s, 12 H, *o*-C*H*$_3$ Mes), 2.28 (s, 6 H, *p*-C*H*$_3$ Mes), 2.53-2.75 (m, 4 H, PC*H*$_2$C*H*$_2$), 2.98 (b, 1 H, O*H*), 3.67 (t, 2 H, $^{3}J_{HH}$ = 4.5 Hz, C*H*$_2$OH), 4.20 (m, 2 H, $^{3}J_{HH}$ = 5.1 Hz OC*H*$_2$), 6.86 (s, 4 H, *H*$_{ar}$ Mes);

^{31}P{^{1}H} NMR (121.49 MHz, $CDCl_3$, 298 K): δ [ppm] = 24.8 ppm;

^{13}C{^{1}H} NMR (75.47 MHz, $CDCl_3$, 298 K): δ [ppm] = 19.9 (s, *o*-*C*H$_3$ Mes), 21.4 (s, *p*- *C*H$_3$ Mes), 21.7 (d, $^{1}J_{PC}$ = 54.8 Hz, *C*H$_2$P), 26.9 (d, $^{2}J_{PC}$ = 4.2 Hz, *C*H$_2$CO), 60.7 (s, OCO*C*H$_2$), 67.1 (s, *C*H$_2$OH), 129.5 (s, *C*^{3,5} Mes), 135.7 (d, $^{2}J_{PC}$ = 41.4 Hz, *C*^{1} Mes), 136.0 (s, *C*^{2,6} Mes), 141.8 (s, *C*^{4} Mes), 171.6 (d, $^{3}J_{PC}$ = 8.2 Hz, *C*OCH$_2$), 215.2 (d, $^{1}J_{PC}$ = 53.7 Hz, *C*OMes);

IR (ATR [cm^{-1}]): 2951 (w), 1743 (m), 1672 (m), 1643 (m), 1604 (m), 1182 (s), 1070 (m), 1042 (m);

ESI MS $[M + H]^+$ m/z = 459.1931, meas. 459.1928;

m.p. 78°C.

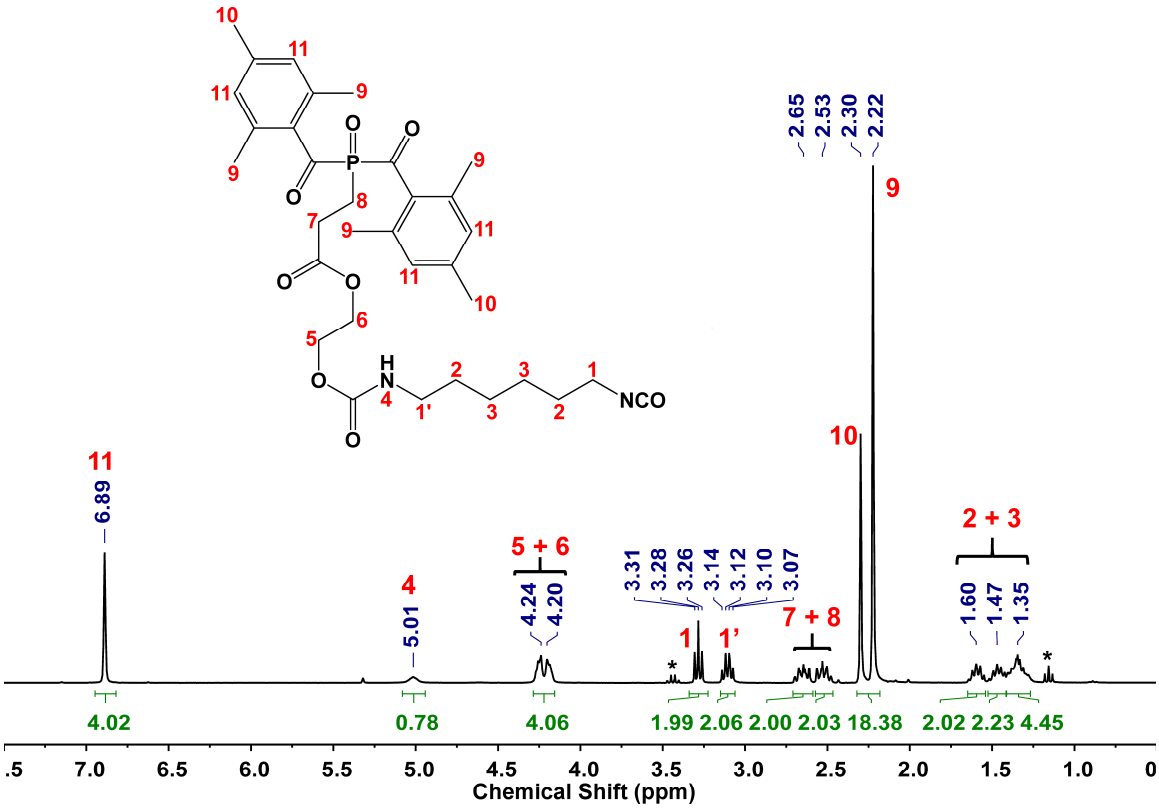

Figure S2a. ^{1}H NMR spectrum of BAPO-NCO (**5**) in CD_2Cl_2 (* is diethyl ether).

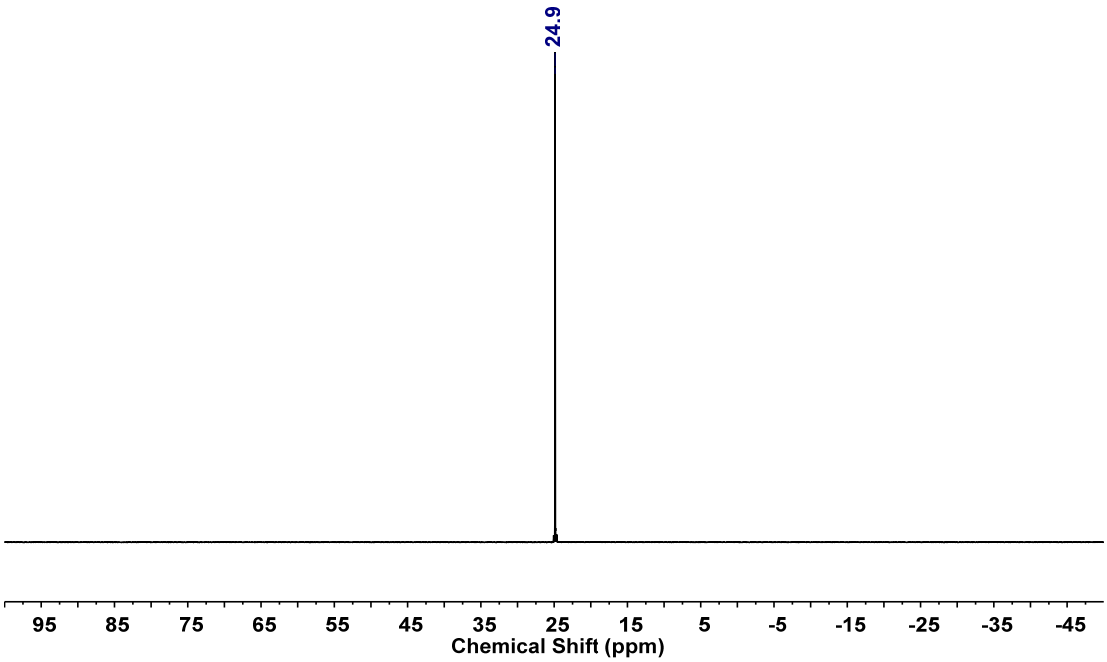

Figure S2b. $^{31}P\{^{1}H\}$ NMR spectrum of BAPO-NCO (**5**) in CD_2Cl_2.

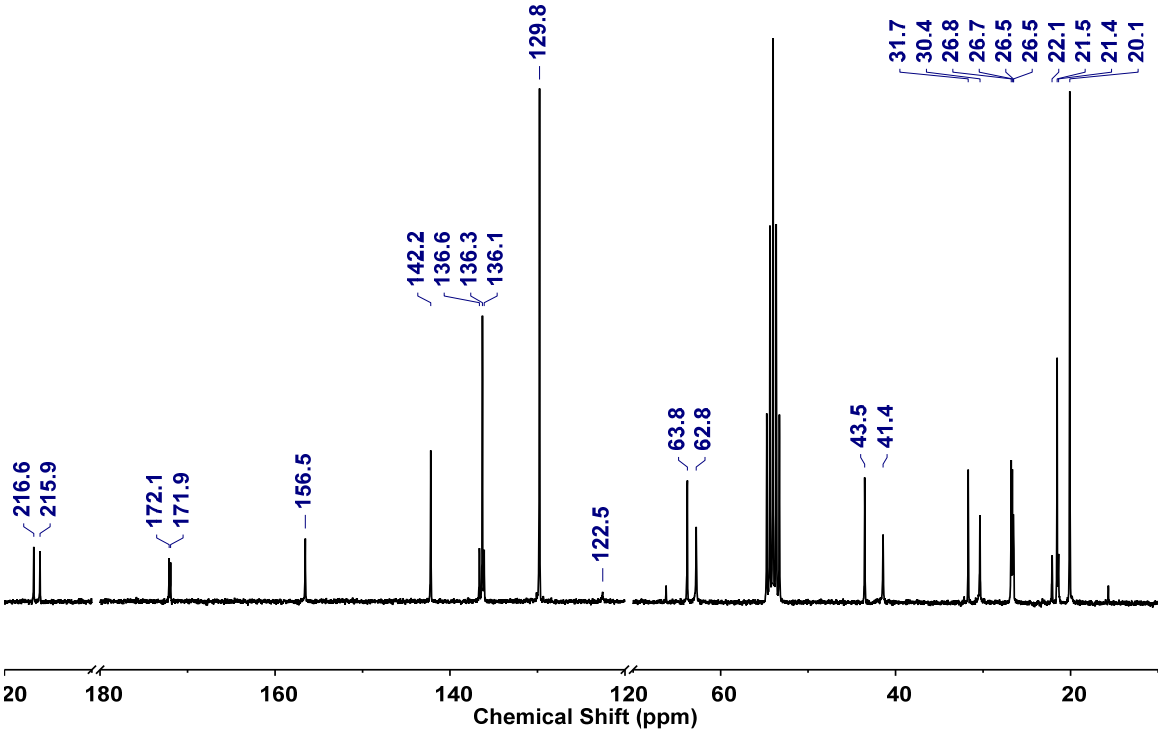

Figure S2c. $^{13}C\{^{1}H\}$ NMR spectrum of BAPO-NCO (**5**) in CD_2Cl_2.

Characterization of 2-([{6-isocyanatohexyl}carbamoyl]oxy)ethyl 3-(bis(2,4,6-trimethylbenzoyl) phosphoryl)propanoate (5)

^{1}H NMR (300.13 MHz, CD_2Cl_2, 298 K): δ [ppm] = 1.26-1.41 (m, 4 H, C*H*$_2$C*H*$_2$CH$_2$CH$_2$NCO), 1.41-1.53 (m, 2 H, C*H*$_2$CH$_2$NH), 1.53-1.66 (m, 2 H, C*H*$_2$CH$_2$NCO), 2.22 (s, 12 H, *o*-C*H*$_3$ Mes), 2.30 (s, 6 H, *p*-C*H*$_3$ Mes), 2.47-2.57 (m, 2 H, PC*H*$_2$CH$_2$), 2.60-2.71 (m, 2 H, PCH$_2$C*H*$_2$), 3.11 (q, 2 H, C*H*$_2$NH), 3.28 (t, 2 H, $^{3}J_{HH}$ = 6.6 Hz, C*H*$_2$NCO), 4.15-4.22 (m, 2 H, C*H*$_2$OCONH), 4.22-4.30 (m, 2 H, C*H*$_2$OCOCH$_2$), 5.01 (b, 1 H, N*H*), 6.89 (s, 4 H, *H*$_{ar}$ Mes);

^{31}P{^{1}H} NMR (121.49 MHz, CD_2Cl_2, 298 K): δ [ppm] = 24.9 ppm;

^{13}C{^{1}H} NMR (75.47 MHz, CD_2Cl_2, 298 K): δ [ppm] = 20.1 (s, *o*-*C*H$_3$ Mes), 21.5 (s, *p*-*C*H$_3$ Mes), 21.7 (d, $^{1}J_{PC}$ = 55.5 Hz, *C*H$_2$P), 26.5 (d, $^{2}J_{PC}$ = 2.9 Hz, *C*H$_2$CO), 26.7 (s, *C*H$_2$CH$_2$CH$_2$NH), 26.8 (s, *C*H$_2$CH$_2$CH$_2$NCO), 30.4 (s, *C*H$_2$CH$_2$NH), 31.7 (s, *C*H$_2$CH$_2$NCO), 41.4 (s, *C*H$_2$NH), 43.5 (s, *C*H$_2$NCO), 62.8 (s, *C*H$_2$OCONH), 63.8 (s, *C*H$_2$OCOCH$_2$), 122.5 (s, N*C*O), 129.8 (s, *C*^{3,5} Mes), 136.3 (s, *C*^{2,6} Mes), 136.4 (d, $^{2}J_{PC}$ = 41.1 Hz, *C*^{1} Mes), 142.2 (s, *C*^{4} Mes), 172.0 (d, $^{3}J_{PC}$ = 12.6 Hz, *C*OCH$_2$), 216.3 (d, $^{1}J_{PC}$ = 53.5 Hz, *C*OMes);

IR (ATR [cm^{-1}]): 2929 (w), 2895 (w), 2259 (s), 1738 (m), 1712 (s), 1680 (s), 1606 (m), 1542 (m), 1254 (m), 1197 (s), 1142 (s);

ESI MS [M + NH$_4$]$^{+}$ m/z = 644.3095, meas. 644.3089;

m.p. 61°C.

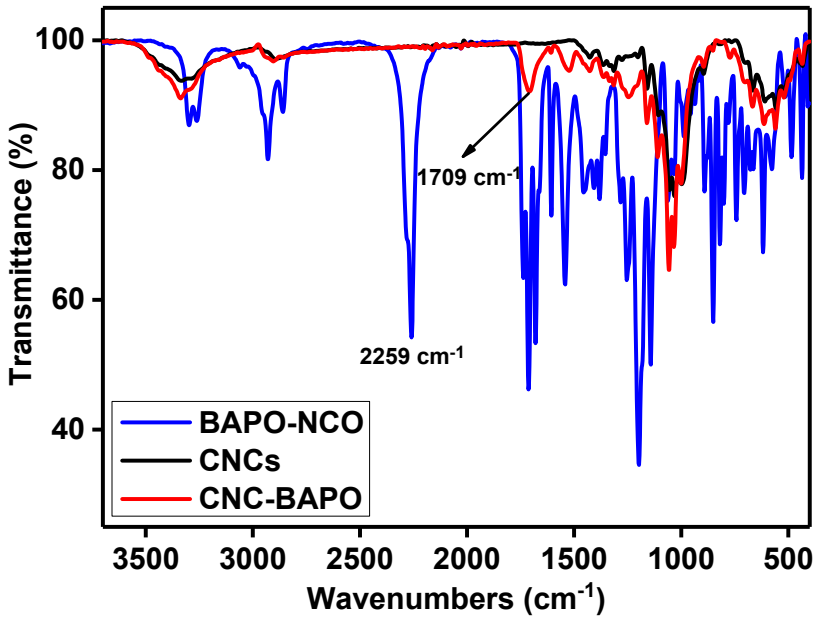

Figure S3. FTIR-ATR spectra of BAPO-NCO, neat CNCs and CNC-BAPO.

In the spectrum of BAPO-NCO, the strong absorbance of the isocyanate group at 2259 cm^{-1} is clearly observed.

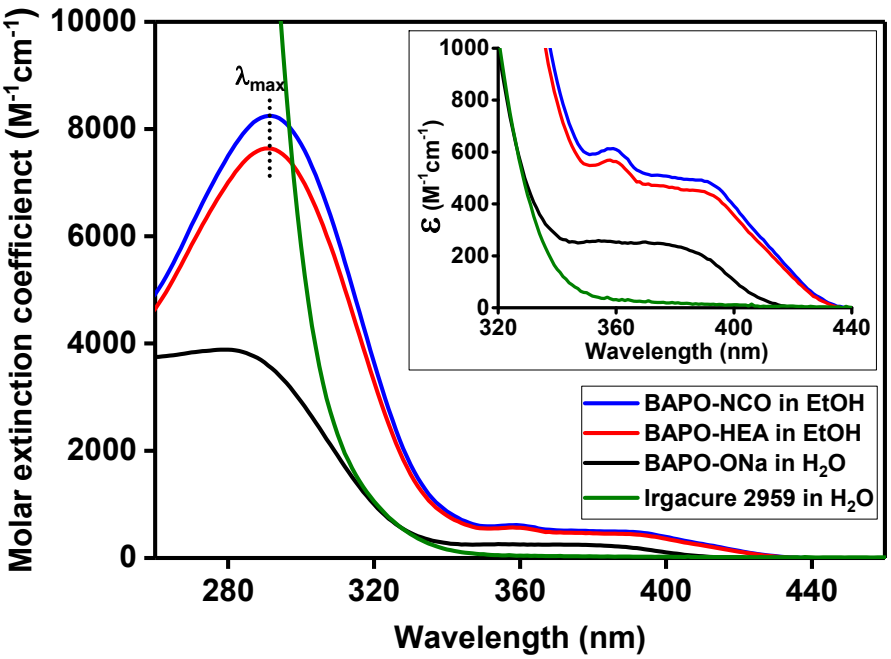

Figure S4. UV-Vis absorption spectra of BAPO-HEA, BAPO-NCO, BAPO-ONa and Irgacure 2959 in different solvents recorded at the same concentrations (0.1 mM).

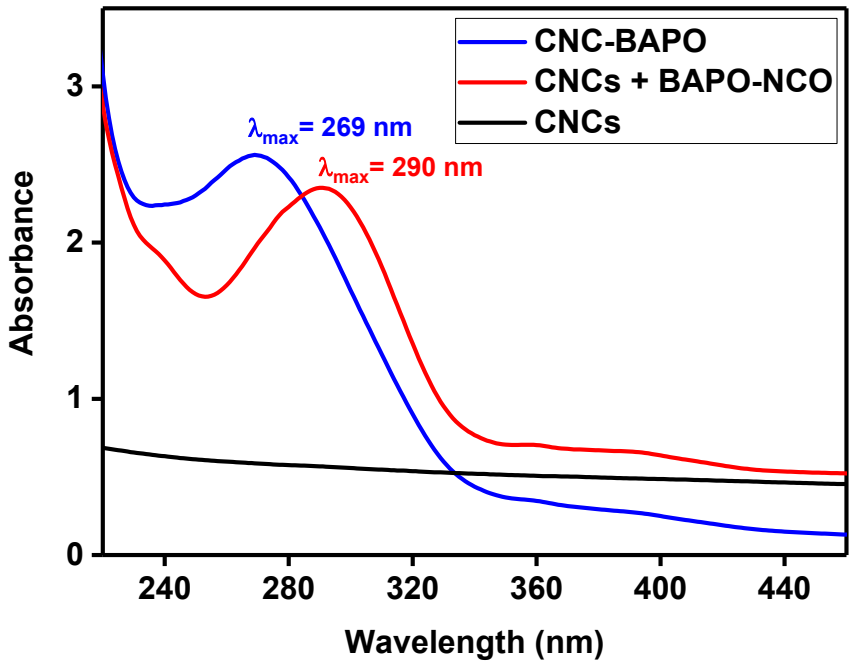

Figure S5. UV-Vis absorption spectra of neat CNCs (288 µg/mL), a blend of BAPO-NCO and neat CNCs (containing 72 µg of BAPO-NCO and 288 µg of neat CNCs per mL), and CNC-BAPO (360 µg/mL) in ethanol. The amounts of CNCs and BAPO-NCO were calculated based on the phosphorus content determined by elemental analysis of the CNC-BAPO sample.

The wavelength of maximum absorbance (λ_{max}, $\pi \rightarrow \pi^*_{CO}$) of CNC-BAPO is blue shifted compared to a physical blend of BAPO-NCO and neat CNCs (λ_{max} = 290 nm) by 21 nm to 269 nm.

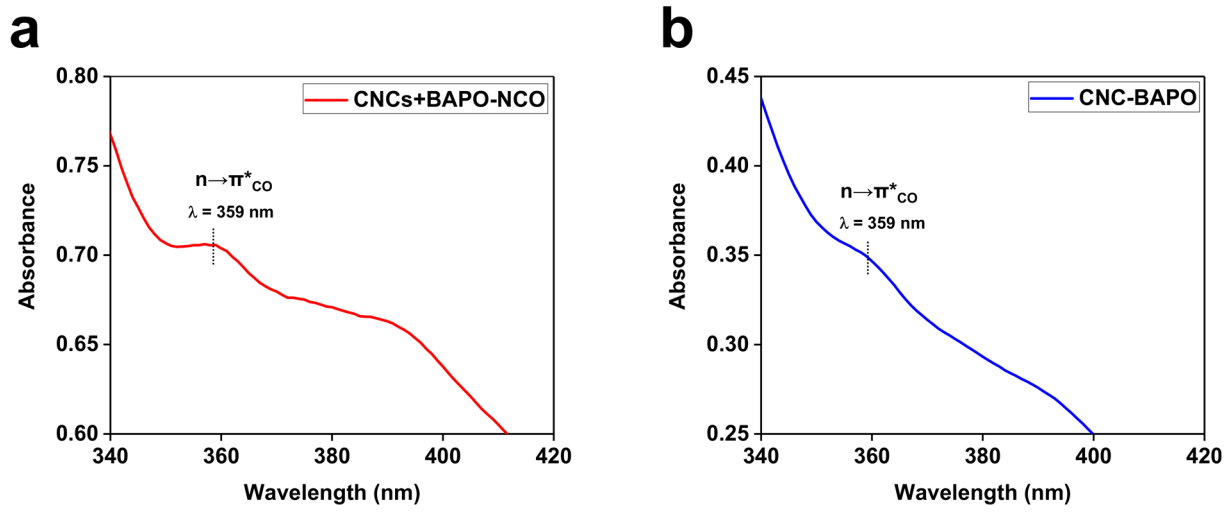

Figure S6. UV-Vis absorption spectra in the selected range from 340 nm to 420 nm. (**a**) The physical blend of BAPO-NCO and CNCs. (**b**) CNC-BAPO.

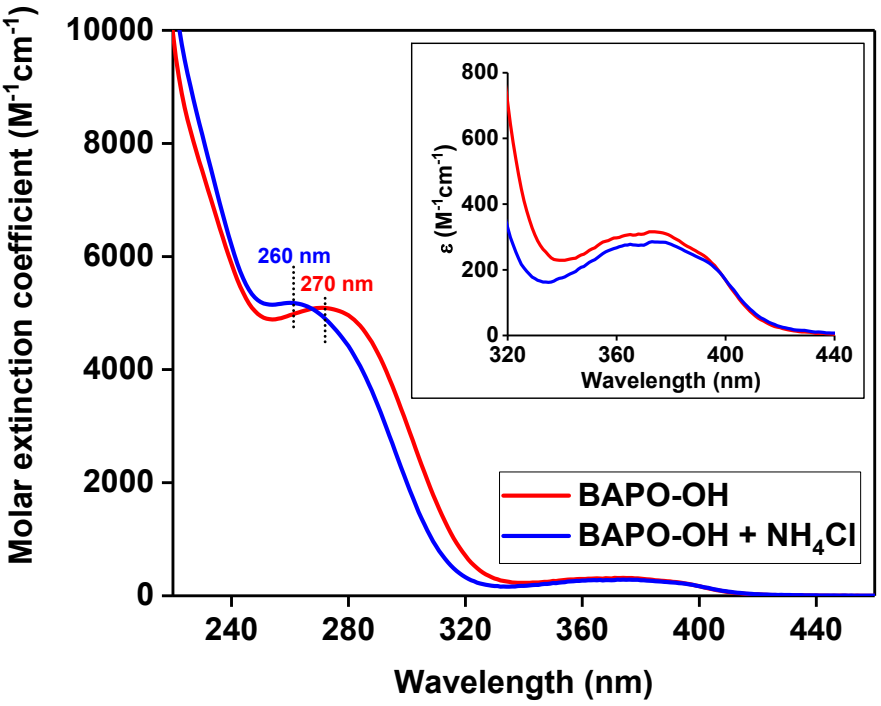

Figure S7. UV-Vis absorption spectra of BAPO-OH mixed with (blue line) and without NH_4Cl (red line) in ethanol recorded at a concentration of 0.1 mM.

The blue shift is supported by an experiment in which BAPO-OH (**7a**) was mixed with NH_4Cl which also leads to a blue shift of the $\pi \rightarrow \pi^*_{CO}$ transition while the $n \rightarrow \pi^*_{CO}$ band remains unaffected.

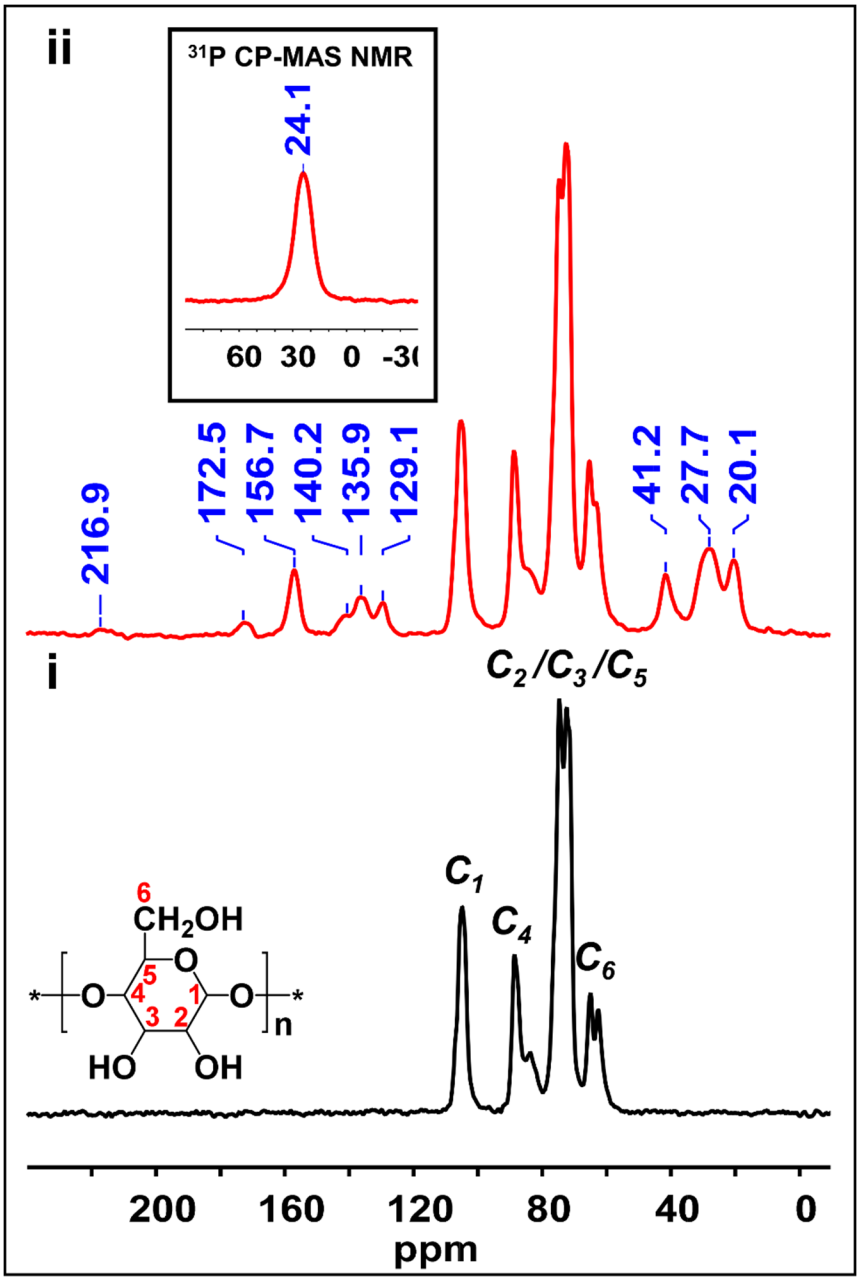

Figure S8. ^{13}C CP-MAS NMR spectrum of unmodified CNCs (**i**), ^{13}C and ^{31}P CP-MAS NMR spectra of CNC-BAPO (**ii**).

Typical ^{13}C signals of cellulose nanocrystals at δ = 105.0 (C_1), 88.6 (C_4 crystalline), 83.8 (C_4 amorphous), 74.7/72.4 ($C_{2,3,5}$), 65.0 (C_6 crystalline), and 62.9 ppm (C_6 amorphous) are observed in both spectra.

The characteristic signals of the BAPO units at δ = 216.9 (*C*OMes), 172.5 (*C*OCH_2), 156.7 (*C*ONH), 140.2 (C^4 Mes), 135.9 ($C^{2,6}$ Mes), 129.1 ($C^{3,5}$ Mes), 41.2 and 27.7 (CH_2 chains of HDI), and 20.1 ppm (*o, p*-CH_3 Mes) are clearly identifiable.

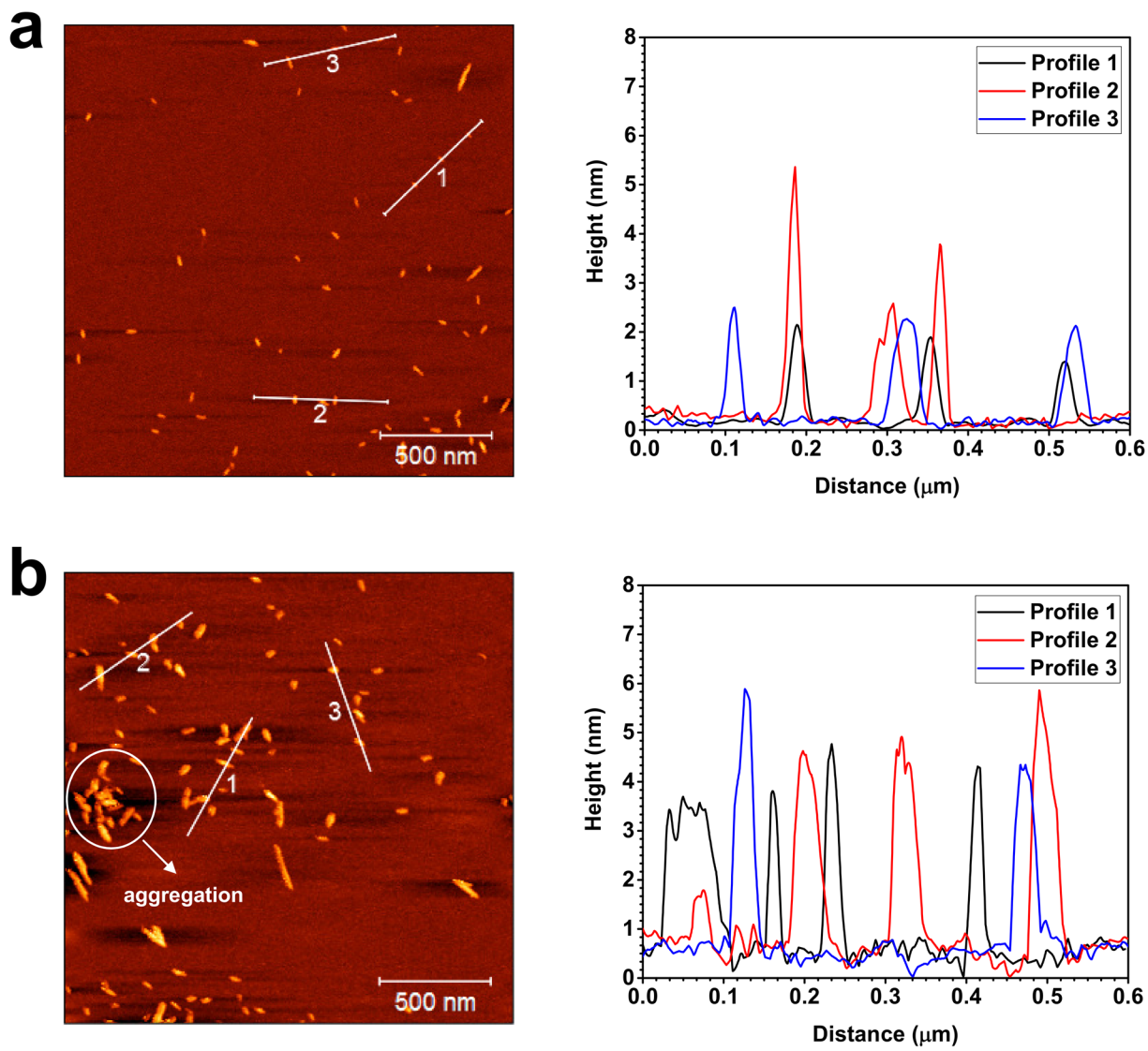

Figure S9. Tapping mode AFM 2 × 2 μm height images and height analysis of individual nanocrystals: unmodified CNCs (**a**) and CNC-BAPO (**b**).

A slight aggregation was detected, since the introduced hydrophobic BAPO units can decrease the dispersity of cellulose nanocrystals in water.

The height of BAPO functionalized CNCs are similar to the unmodified CNCs. Please notice that AFM heights are almost half as large as TEM widths (an average diameter of 5–10 nm and lengths of 100–150 nm, data from the University of Maine) which might be due to counting of a larger fraction of laterally associated CNCs in the TEM images.[4]

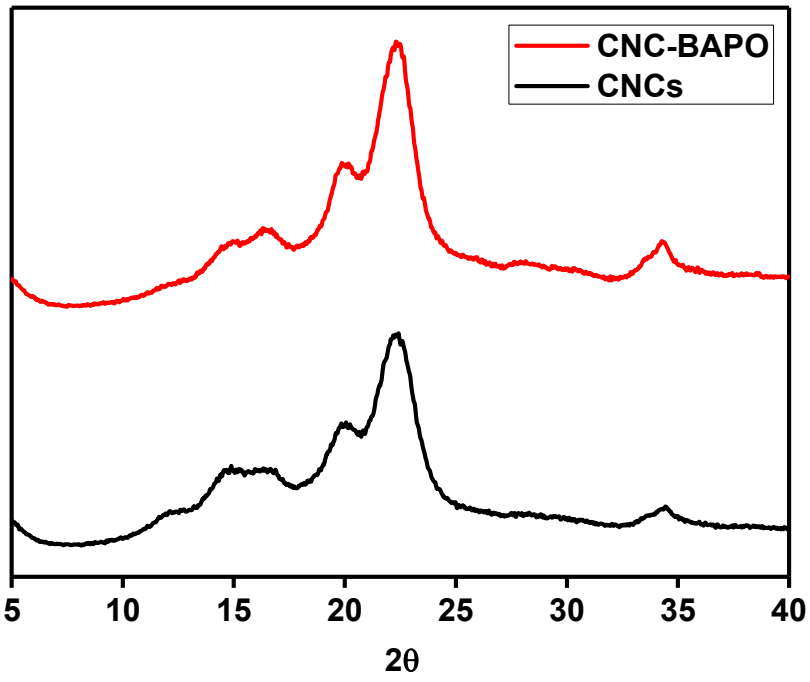

Figure S10. X-ray diffraction patterns of unmodified CNCs and CNC-BAPO.

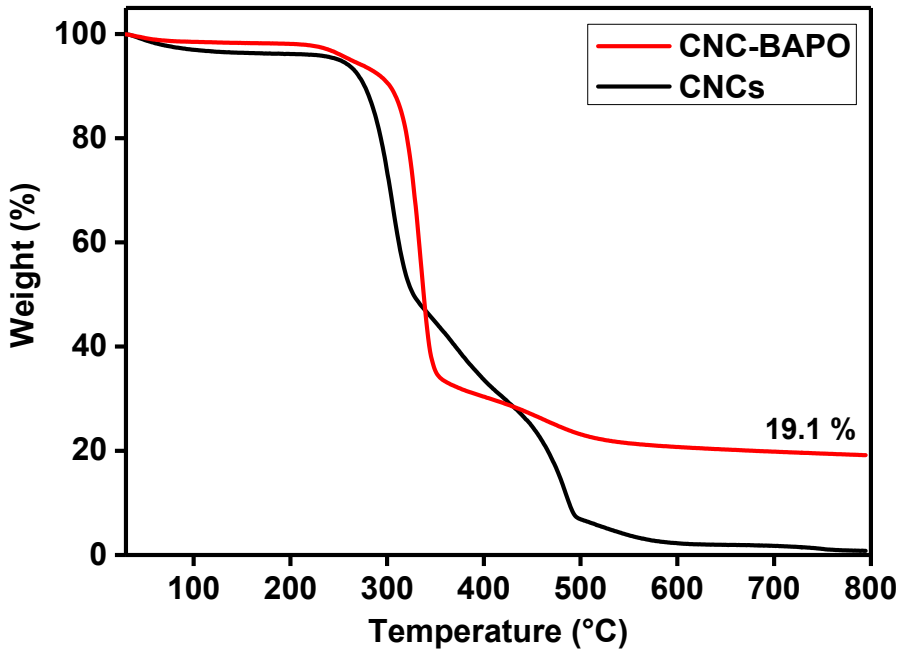

Figure S11. TGA thermograms of unmodified CNCs and CNC-BAPO.

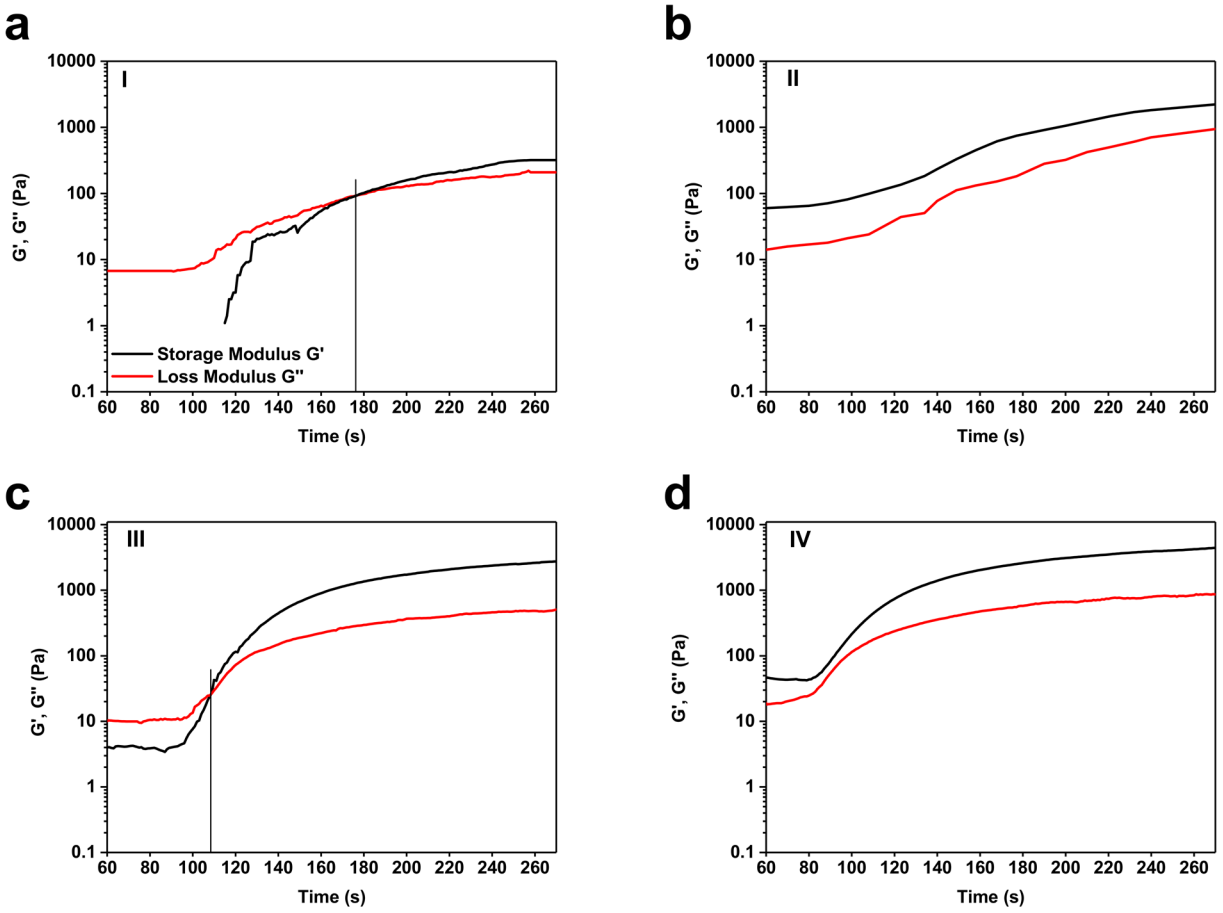

Figure S12. Time dependence of storage modulus *G'* and loss modulus *G"* for formulations: (**a**) formulation **I**; (**b**) formulation **II**; (**c**) formulation **III**; (**d**) formulation **IV**. The light was switched on 60 seconds after the recording of data started. The data shown here are obtained after this delay.

For samples **I** and **III**, *G'* is lower than *G"* before irradiation, as it is common for liquid formulations. In these two graphs, the gel points were observed and it is evident that with the use of CNC-BAPO, the gel point,[5] which is generally defined as the time required for *G'* to surpass *G"*, is reached in a shorter time. For samples **II** and **IV**, the physical interactions among cellulose nanocrystals and the monomers in water are high and these formulations gave already "gelly" materials (*G'* > *G"*) before irradiation. Therefore, a gel point could not be observed.

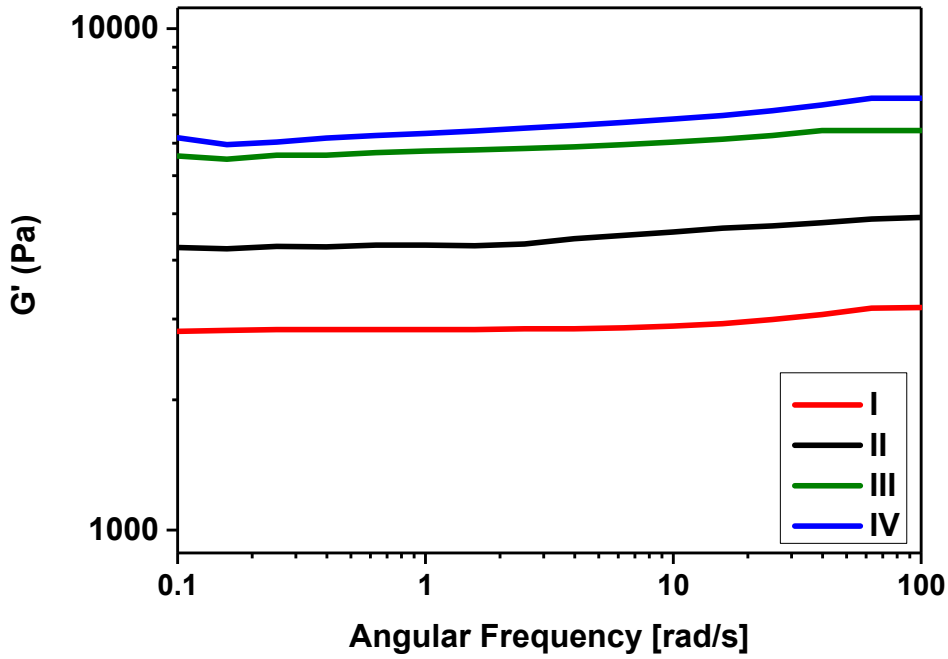

Figure S13. Frequency sweep measurements performed on specimens irradiated in the photorheometer.

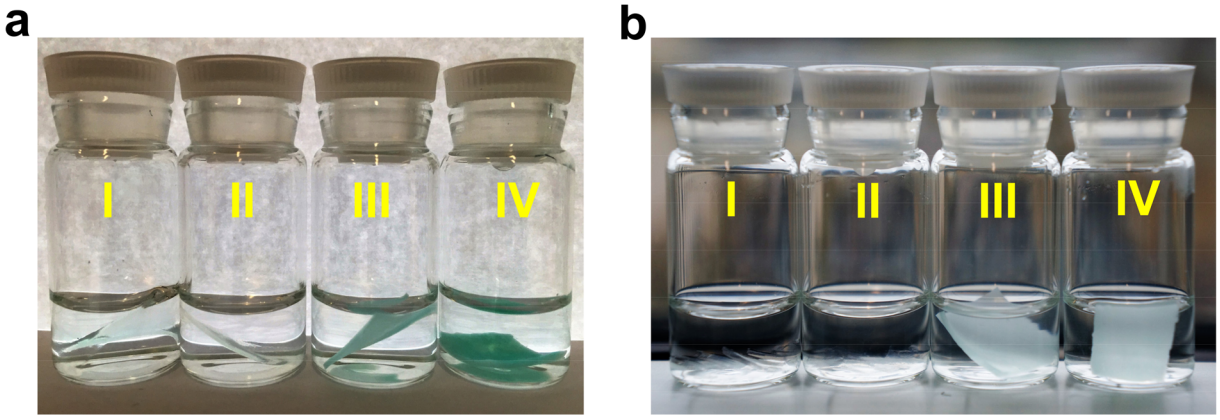

Figure S14. Photographs of casted films (0.5 mm thick) obtained from formulations according to Table 1 after placing them in deionized water for 5 min (**a**) and after immersion in water for 24 h followed by 30 min sonication (**b**).

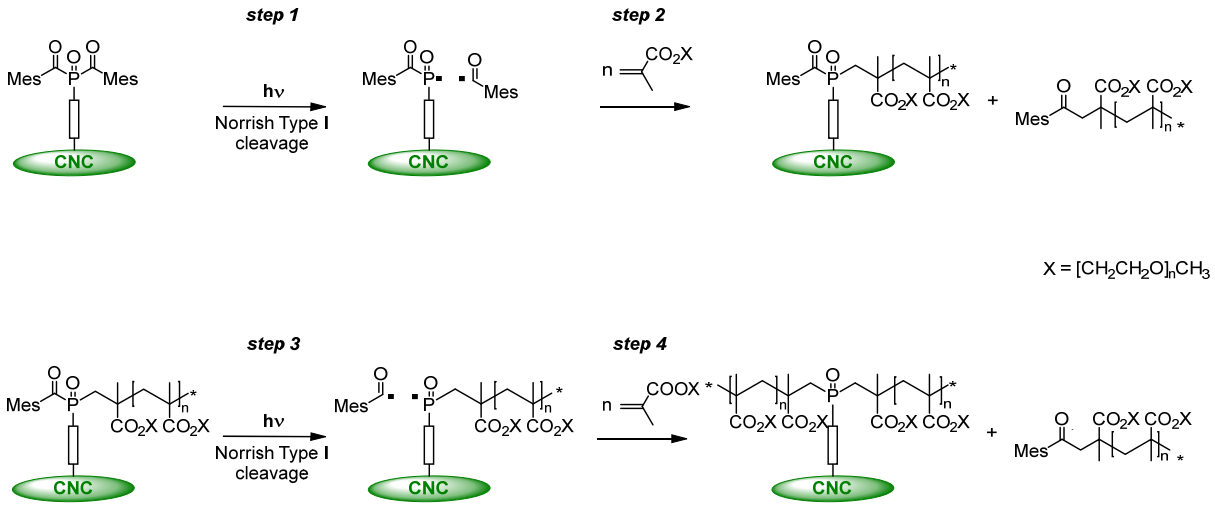

Figure S15. Detailed schematic representation of the polymerization process initiated by surface bound bis(acyl)phosphane oxides.

In each of the reaction steps (1) and (3), a phosphorus centered radical is formed, which is chemically linked to the CNCs surfaces. Both radicals, which are generated in two subsequent photoinitiated cleavage reactions, efficiently initiate the polymerization of acrylic double bonds, resulting in two polymer chains growing from the surface-fixed phosphorus atom (reaction steps (2) and (4)). In the same photoinduced cleavage reactions (1) and (3), two mesitoyl radicals are concomitantly formed, which are not linked to the substrate. Although mesitoyl radicals are known to be less efficient in the initiation of acrylate polymerization than the phosphinoyl radicals, this inevitably leads to the formation of nonbound homopolymers as shown in both reaction steps (2) and (4). These linear photopolymers can, however, easily be removed from the grafted CNCs surfaces by careful washing with water.

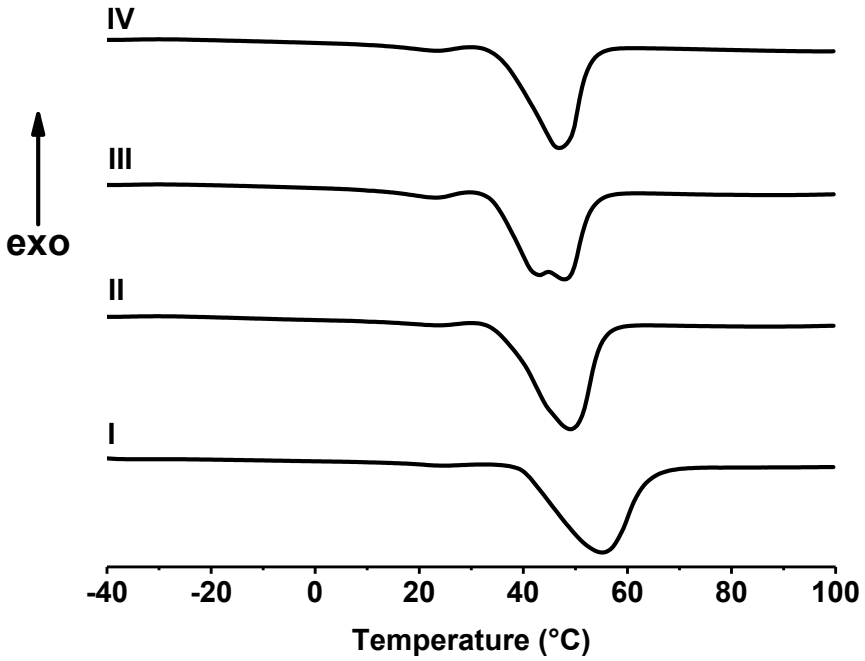

Figure S16. DSC thermograms of the thin films obtained.

A second melting peak appears at lower temperature in **III**. This can be attributed to different thickness of crystals owing to the varying number of folds in the polymer chain.[6]

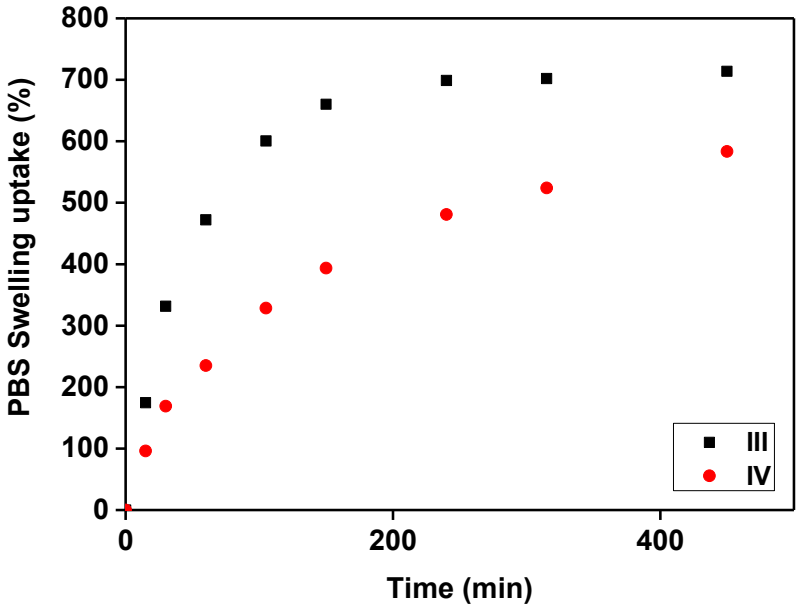

Figure S17. Swelling kinetics of the dried printed samples at room temperature in PBS.

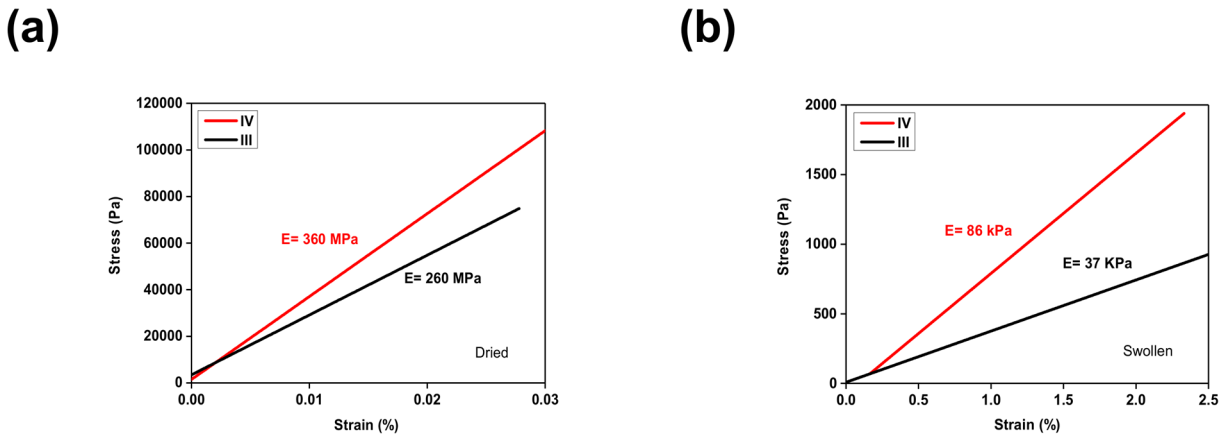

Figure S18. Tensile tests performed on the 3D printed samples: dried (**a**) and swollen (**b**).

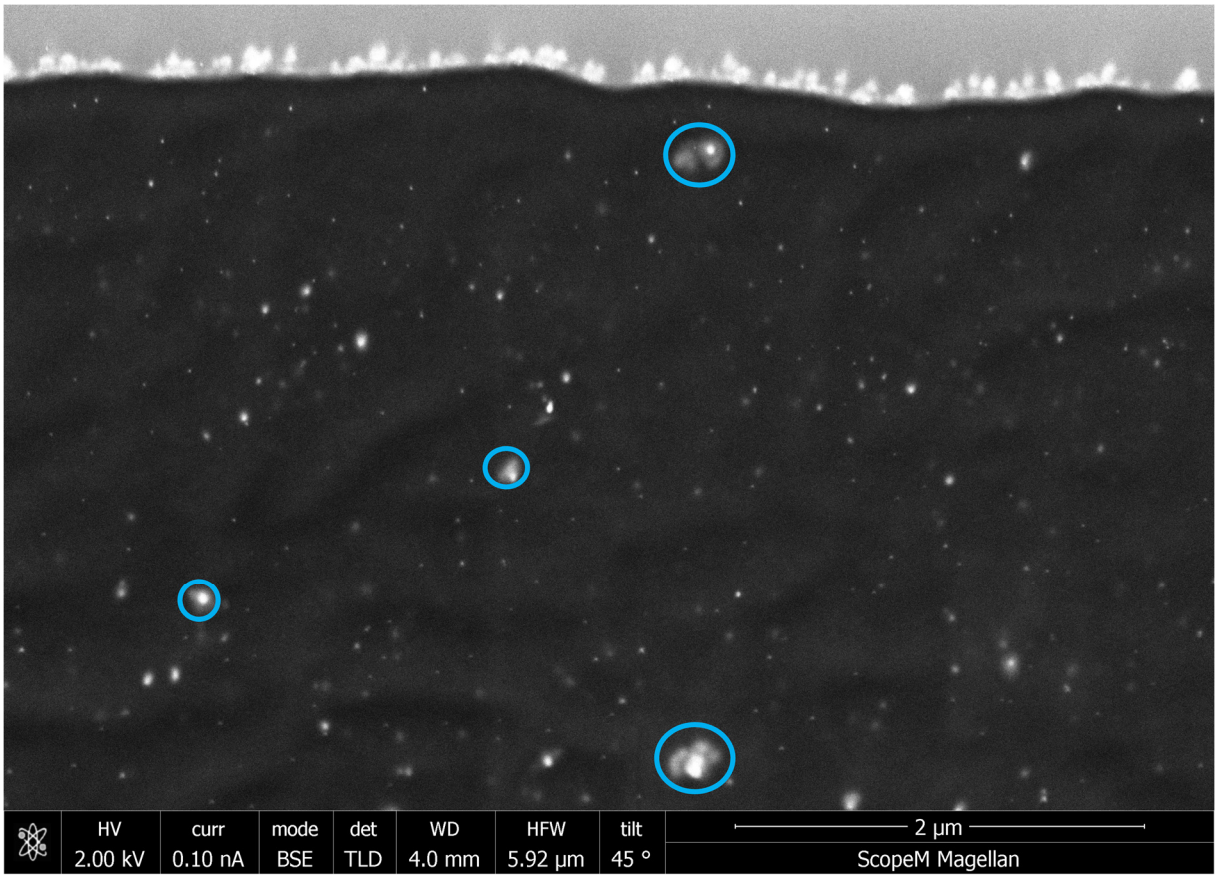

Figure S19. SEM images of a 3D printed thin film with the formulation **IV**.

Small white dots which have been previously reported[7] indicate the cross-sections of individual cellulose nanocrystals distributed in the nanocomposite hydrogels. Blue circles suggest aggregates are formed.

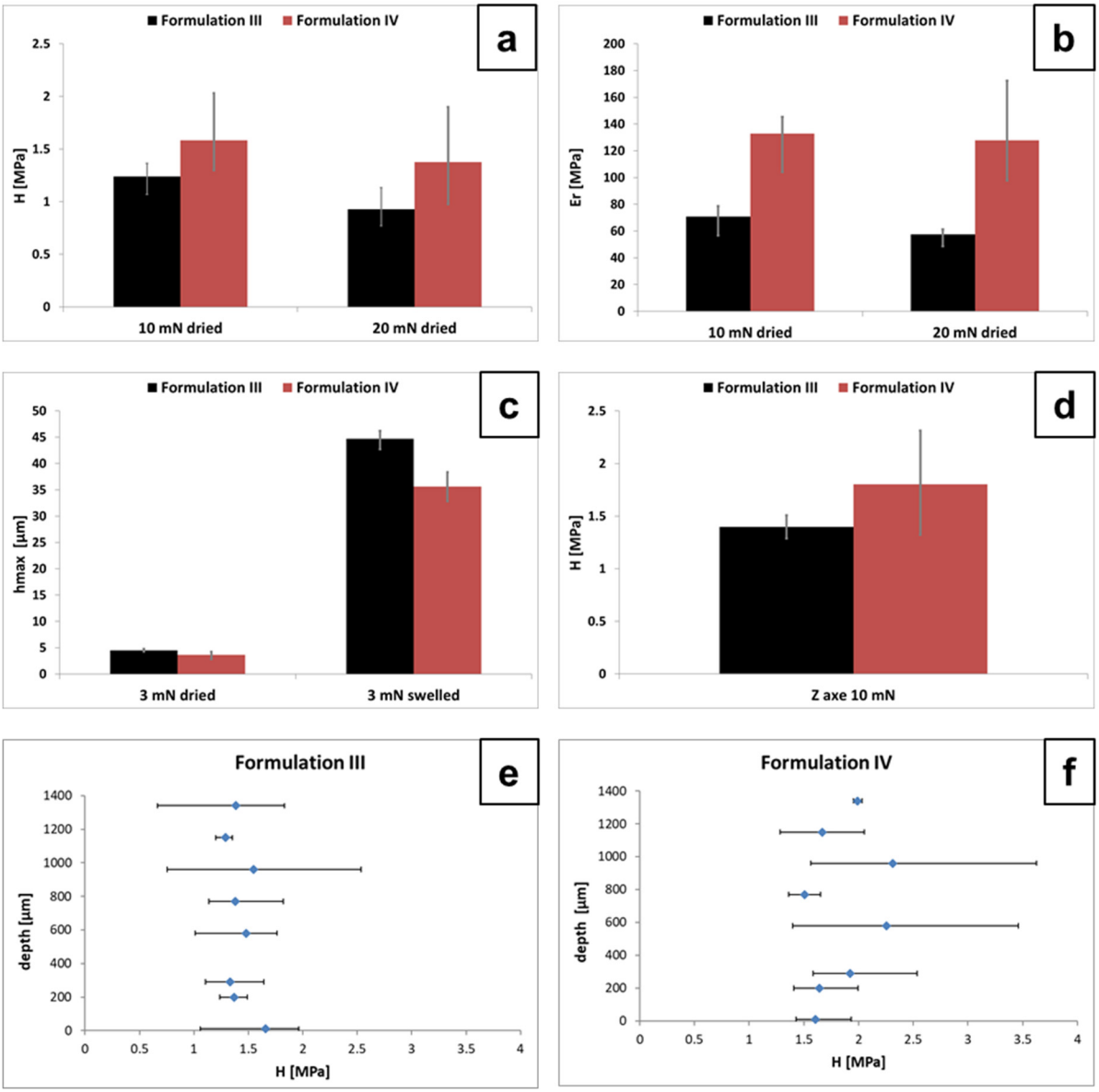

Figure S20. Hardness (**a**) and reduced elastic modulus (**b**) values of dried samples of formulation **III** and **IV**; maximum depth values of dried and swollen samples of **III** and **IV** (**c**); hardness values on Z axis planes of samples of **III** and **IV** (**d**); hardness values along Z axis at different depth on **III** (**e**) and **IV** (**f**).

Estimation of the number of BAPO-NCO units bound on one CNC

The cellulose nanocrystals exhibit an average diameter of 5–10 nm and lengths of 100–150 nm as declared by the material supplier at the University of Maine.

Under the assumption that a nanocrystal has a rod-like form,[8] the volume V_{CNC} of a single nanocrystal is given by:

$$V_{CNC} = \frac{\pi}{4} d^2 l$$

d = average width of the nanocrystals = 8 nm;

l = average length of the nanocrystals = 125 nm.

Mass, m_{CNC}, of a single nanocrystal:

$$m_{CNC} = V_{CNC} \times \rho$$

ρ = density of the nanocrystals = 1.5 g/cm^3 (density of crystalline cellulose[4]).

Numbers, n_{CNC}, of nanocrystals in 1 g CNCs:

$$n_{CNC} = \frac{1}{m_{CNC}}$$

The weight content, m_{BAPO}, of BAPO-NCO grafted onto 1 g of CNC-BAPO is given by:

$$m_{BAPO} = \frac{1 \times E_P}{M_P} \times M_{BAPO}$$

E_P = phosphorus content of the sample = 0.94% as determined by elemental analysis;

M_P = molecular weight of phosphorus = 31 g·mol^{-1};

M_{BAPO} = molecular weight of the BAPO-NCO = 626.7 g·mol^{-1}.

Number, n_{BAPO}, of BAPO-NCO molecules grafted onto 1 g of CNC-BAPO:

$$n_{BAPO} = \frac{m_{BAPO}}{M_{BAPO}} \times N_A$$

N_A = Avogadro constant = 6.022×10^{23} mol^{-1}

Mass of CNCs in 1 g of CNC-BAPO:

$$m_{CNC-BAPO} = 1 - m_{BAPO}$$

Numbers of CNCs, $n_{CNC\text{-}BAPO}$, in 1g of CNC-BAPO:

$$n_{CNC-BAPO} = n_{CNC} \times \frac{m_{CNC-BAPO}}{1}$$

The ratio between BAPO-NCO and CNCs in 1 g of CNC-BAPO:

$$R = \frac{n_{BAPO}}{n_{CNC-BAPO}} = \frac{E_P \times N_A}{M_P} \times \frac{m_{CNC}}{m_{CNC-BAPO}} = \frac{E_P \times N_A}{M_A} \times \frac{V_{CNC} \times \rho}{1 - m_{BAPO}} \approx 2.1 \times 10^3$$

Surface density calculation, ρ_A, of BAPO-NCO units on one single nanocrystal:

$$\rho_A = \frac{m_{BAPO}}{A_{CNC-BAPO}} = \frac{m_{BAPO}}{\frac{4}{\rho \times d} \times m_{CNC-BAPO}} \approx 7.0 \times 10^{-8}\, g / cm^2$$

References

[1] M. Labet, W. Thielemans, *Cellulose* **2011**, *18*, 607-617.

[2] A. Chiappone, S. Jeremias, R. Bongiovanni, M. Schönhoff, *Journal of Polymer Science Part B: Polymer Physics* **2013**, *51*, 1571-1580.

[3] W. C. Oliver, G. M. Pharr, *Journal of Materials Research* **1992**, *7*, 1564-1583.

[4] A. Brinkmann, M. Chen, M. Couillard, Z. J. Jakubek, T. Leng, L. J. Johnston, *Langmuir* **2016**, *32*, 6105-6114.

[5] R. Muller, E. Gerard, P. Dugand, P. Rempp, Y. Gnanou, *Macromolecules* **1991**, *24*, 1321-1326.

[6] Wunderlich, B. “Macromolecular physics”, Vol. 2: *Crystal Nucleation, Growth Annealing*, Academics Press, New York, **1976**.

[7] L. Tang, C. Weder, *ACS Applied Materials & Interfaces* **2010**, *2*, 1073-1080.

[8] G. Siqueira, J. Bras, A. Dufresne, *Langmuir* **2010**, *26*, 402-411.